IEEE Photonics Journal
An IEEE Photonics Society Publication

Open Access

Widely Tunable Semiconductor Laser Based on Digital Concatenated Grating With Multiple Phase Shifts

Volume 5, Number 5, October 2013

Jialin Zhao
Sheng Hu
Yichao Tang
Hang Zhao
Yonglin Yu, Member, IEEE

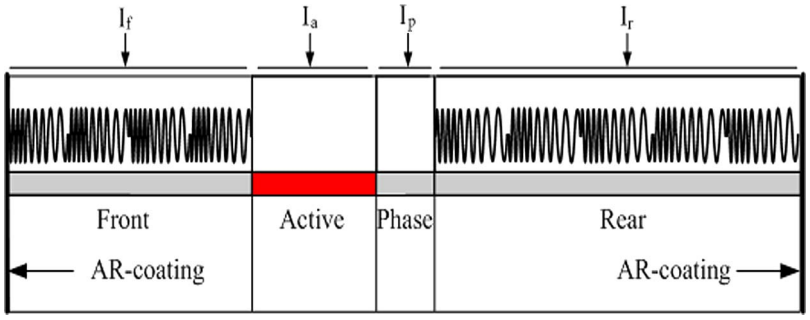

DOI: 10.1109/JPHOT.2013.2278514
1943-0655

IEEE photonics SOCIETY

IEEE

Widely Tunable Semiconductor Laser Based on Digital Concatenated Grating With Multiple Phase Shifts

Jialin Zhao, Sheng Hu, Yichao Tang, Hang Zhao, and Yonglin Yu, *Member, IEEE*

Wuhan National Laboratory for Optoelectronics, School of Optical and Electronic Information, Huazhong University of Science and Technology, Wuhan 430074, China

DOI: 10.1109/JPHOT.2013.2278514

Manuscript received April 25, 2013; revised August 7, 2013; accepted August 8, 2013. Date of publication August 15, 2013; date of current version October 1, 2013. This work was supported in part by the International S&T Cooperation Program of China under Grant 1016, by the National Natural Science Foundation of China under Grant 11174097, and by the Specialized Research Fund for the Doctoral Program of Higher Education (SRFDP) under Grant 20100142110045. Corresponding author: Y. Yu (e-mail: yonglinyu@mail.hust.edu.cn).

Abstract: In this paper, we proposed a widely tunable distributed Bragg reflector (DBR) laser based on digital concatenated grating with multiple phase shifts (MPS-DCG). The MPS-DCG can provide a comblike reflectivity spectrum with flat envelop covering over 100-nm wavelength range. Static characteristics of the MPS-DCG DBR laser, including the wavelength tuning range, output power, side-mode suppression ratio (SMSR), and $L-I$ curves, are simulated using a time-domain traveling-wave model combined with a digital filter method. Tuning range of approximately 90 nm is obtained with good SMSR. The $L-I$ curves show that the laser threshold current is around 30 mA.

Index Terms: Gratings, tunable lasers, modeling, time-domain.

1. Introduction

Widely tunable semiconductor lasers are attractive for various applications in, for example, today's dense wavelength division multiplexed (DWDM) systems and broadband sensors [1]. Tunable lasers are also key components in future optical packet and burst (OPS/OBS) switching systems to reduce the latency and increase the capacity of current optical transmission networks [2], [3]. Several typical tunable lasers have been demonstrated including the sampled-grating (SG) or superstructure grating (SSG) distributed Bragg reflector (DBR) lasers [4], [5], the grating assisted co-directional coupler with rear sampled grating reflector (GCSR) lasers [6], the digital supermode (DS) DBR lasers [7] with phase gratings [8], [9], the binary superimposed grating (BSG) DBR lasers[10] and the modulated grating Y-branch (MGY) lasers [11]. In addition, to provide a "flat-top" comb reflector which is ideal for tunable lasers, we have proposed the wavelength tunable digital concatenated grating (DCG) DBR laser [12].

In this paper, by combining the multiple reflection spectrum concatenation [12] and multiple phase shifts [13] technologies, we proposed a widely tunable four-section DBR laser based on the DCG with multiple phase shifts (MPS-DCG). The static characteristics of the proposed MPS-DCG DBR laser are simulated and analyzed with a time-domain traveling-wave model. The MPS-DCG can provide periodic multiple high reflection peaks in the wavelength range of over 100 nm. Compared to the previous DCG design, the MPS-DCG provides a narrower 3 dB bandwidth of

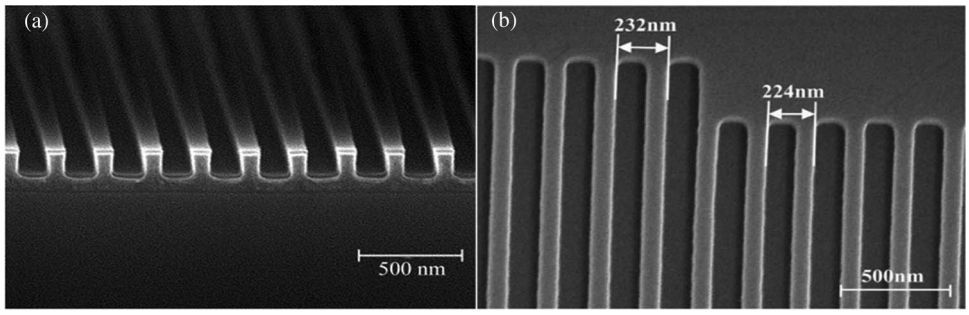

Fig. 1. SEM photographs of the fabricated DCG. (a) DCG pattern on resist after nanoimprint; (b) the ICP etched DCG.

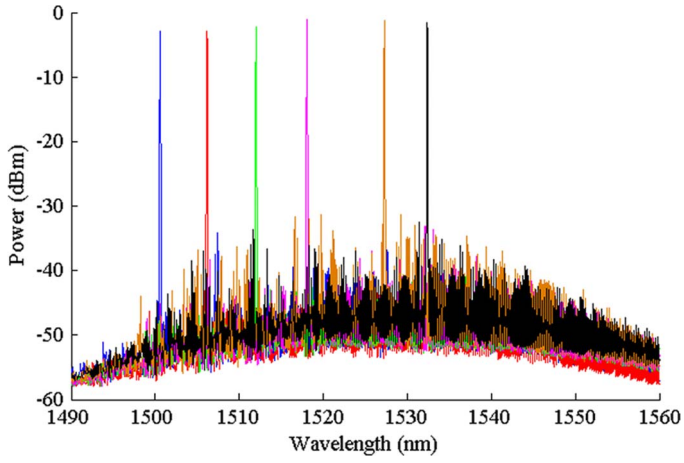

Fig. 2. Superimposed spectra of six DCG-DBR laser supermodes.

reflection peaks which will help to increase mode selectivity. Furthermore, the grating period difference of the MPS-DCG is slightly bigger than that of the DCG, which will help to relieve the stringent requirements on fabrication tolerance of the grating.

2. Grating Design and Laser Structure

To provide a "flat-top" comb reflector for DBR type tunable lasers, we previously proposed a DCG structure [12], and then fabricated the grating by using the nanoimprint lithography (NIL) technology [14]. Fig. 1(a) and (b) show the SEM photography of the DCG pattern on resist after the nanoimprint processing and the inductively coupled plasma (ICP) etched DCG, respectively. In Fig. 1(b), the periods of concatenated grating segments are approximately 224 nm, 228 nm, and 232 nm. In practice, we have to carefully control the fabrication tolerance as the period difference of concatenate Bragg gratings is approximately 4 nm. Besides, the 3 dB bandwidth of reflection peaks of a DCG is not narrow enough, which may result in reduced SMSR and mode instability. This can be observed from the measured lasing spectra of a demonstrated DCG-DBR laser in Fig. 2. Clearly, discrete wavelength tuning of about 32 nm is obtained with six different supermodes. We can see from Fig. 2, although, the SMSRs of these six supermodes are larger than 30 dB, the side modes are not well suppressed possibly due to the relatively large comb reflection peak 3 dB bandwidth of the DCG.

For the above reasons, here we use the multiple phase shifts technology to improve DCG, i.e., MPS-DCG. The schematic structure of the MPS-DCG is shown in Fig. 3. A MPS-DCG consists of M grating segments with different uniform periods, $\Lambda_1, \Lambda_2, \ldots$, and Λ_M in one sampling period. Z_g and

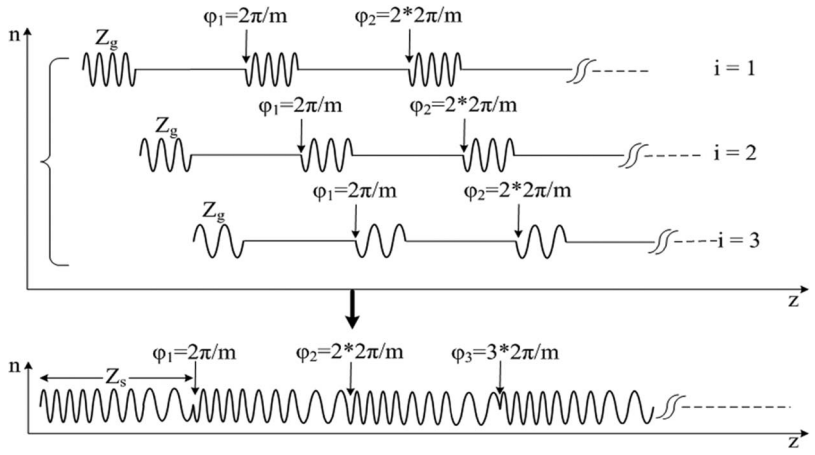

Fig. 3. Schematic structure of a MPS-DCG.

Z_s are length of grating segments and sampling period, respectively, and $Z_s = MZ_g$. The phase shift between the kth and $(k+1)$th sampling period is $\varphi_k = 2\pi k/m$, where m is the phase shift factor. A MPS-DCG consists of M multiple-phase-shifts sampled gratings. By carefully designing MPS sampled grating segments periods, the reflection spectrum envelope of each grating segment is concatenated [15], and by increasing m, channel-counts within the 3 dB reflection envelope bandwidth could be densified. Therefore, by reducing the sampling period Z_s to Z_s/m, the 3 dB bandwidth of reflection spectrum envelope can be increased by a factor of m without changing the peak spacing.

In our design, in order to concatenate the sub-grating reflection spectrum envelope, the Bragg period of the ith sub-grating satisfies the following equations [15]:

$$\Lambda_i - \frac{\lambda_c}{2n_{\text{eff}}} = \begin{cases} \frac{H}{2n_{\text{eff}}}\left(i - \frac{M+1}{2}\right)\Delta\lambda, & m\text{: odd} \\ \frac{H}{2n_{\text{eff}}}\left(i - \frac{M+1}{2}\right)\Delta\lambda + \frac{\Delta\lambda}{4n_{\text{eff}}}, & m\text{: even} \end{cases} \quad i = 1, 2, \ldots, M \tag{1}$$

$$\Delta\lambda = \frac{1}{m}\frac{\lambda_c^2}{2n_{\text{eff}}Z_s} \tag{2}$$

where λ_c is the designed center wavelength of the reflection spectrum, n_{eff} is the effective refractive index, $\Delta\lambda$ is the channel spacing of MPS-DCG and H is a positive coefficient. The optimal H is equal to $m \times M$ to obtain reflection spectrum with wide wavelength range and flat peak reflectivity [15].

Fig. 4 shows the calculated reflection spectra of the MPS-DCG and DCG. The results in Fig. 4(a) indicate that by employing multiple phase shifts technology, the 3 dB bandwidth of reflection spectrum envelope can be increased. When $m = 2$, $M = 3$, multiple reflection peaks are observed in over 120 nm range with a high reflectivity of 60% $\sim$ 80%. The peak 3 dB bandwidths shown in Fig. 4(b) are 0.92 nm and 1.2 nm for MPS-DCG and DCG, respectively. The narrower peak bandwidth of the MPS-DCG has the advantages in good SMSR and mode stability. The corresponding structure parameters of the MPS-DCG and DCG are listed in Table 1. The grating coupling coefficient is 100 cm^{-1}. As shown in this table, the grating period differences between grating segments of the MPS-DCG and DCG are approximately 8.4 nm and 4.2 nm, respectively. As the MPS-DCG has a bigger period difference, it is easier to control in fabrication.

Fig. 5 shows the schematic structure of the wavelength tunable MPS-DCG DBR laser. The MPS-DCG reflectors are formed in the front and rear passive sections. There is a slight difference of reflection peak spacings between the front and rear MPS-DCG reflectors to extend the tuning range based on the Vernier mechanism [4]. The two grating reflectors consist of three grating segments with different Bragg periods in one sampling period, which can be calculated from (1) and (2), and

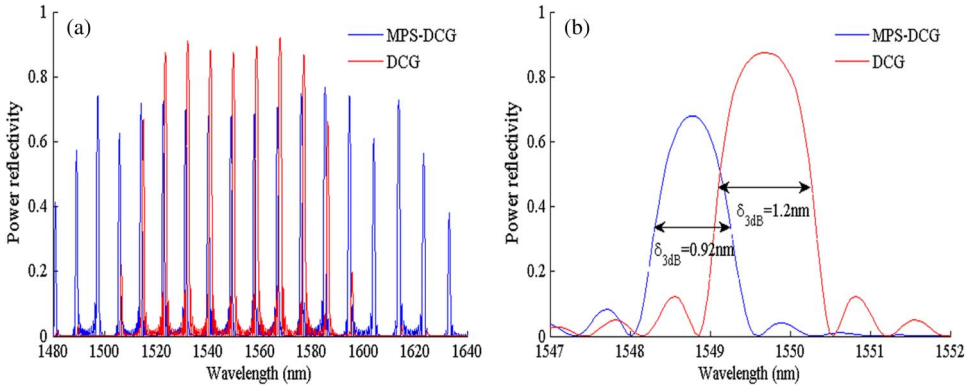

Fig. 4. (a) Reflection spectra of the MPS-DCG, $m = 2$, $M = 3$ and DCG, $M = 3$; (b) Peak 3 dB bandwidth at wavelength around 1550 nm.

TABLE 1
Structure parameters of the MPS-DCG and DCG

MPS DCG			DCG		
The i*th* sub-grating	Bragg Period Λ	Grating segment length Zg	The i*th* sub-grating	Bragg Period Λ	Grating segment length Zg
i=1	232.3 nm	6.97 μm	i=1	235.8 nm	13.9 μm
i=2	240.6 nm	6.97 μm	i=2	239.9 nm	13.9 μm
i=3	249.0 nm	6.97 μm	i=3	244.1 nm	13.9 μm
Sampling Period	20.9 μm		41.7 μm		
Grating length	418.2 μm		417 μm		

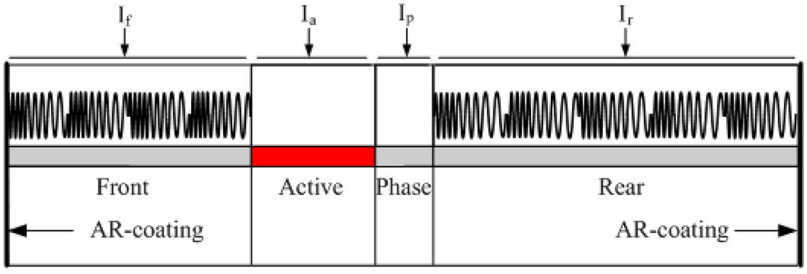

Fig. 5. Schematic structure of the MPS-DCG DBR laser.

the phase shift factor m is chosen to be 2. The structure parameters of the front and rear MPS-DCGs are listed in Table 2, and the grating coupling coefficient is 100 cm^{-1}. The corresponding reflectivities are shown in Fig. 6. This device has a designed tuning range of 88 nm. The length of the active and phase sections are 400 μm and 100 μm, respectively. Both facets of the MPS-DCG DBR laser are AR-coating.

3. Numerical Results and Discussions

The characteristics of the MPS-DCG DBR laser are simulated using the time-domain traveling-wave model [16] combined with a digital filter method [17], [18]. The material and physical parameters used in the simulation are given in Table 3.

TABLE 2

Structure parameters of the front and rear MPS-DCGs

Front grating			Rear grating		
The *ith* sub-grating	Bragg Period Λ	Grating segment length Zg	The *ith* sub-grating	Bragg Period Λ	Grating segment length Zg
i=1	230.7 nm	6.23 μm	i=1	231.6 nm	6.95 μm
i=2	240.0 nm	6.23 μm	i=2	240.0 nm	6.95 μm
i=3	249.2 nm	6.23 μm	i=3	248.3 nm	6.95 μm
Sampling Period	18.7 μm		20.8 μm		
Grating length	224.4 μm		417.2 μm		

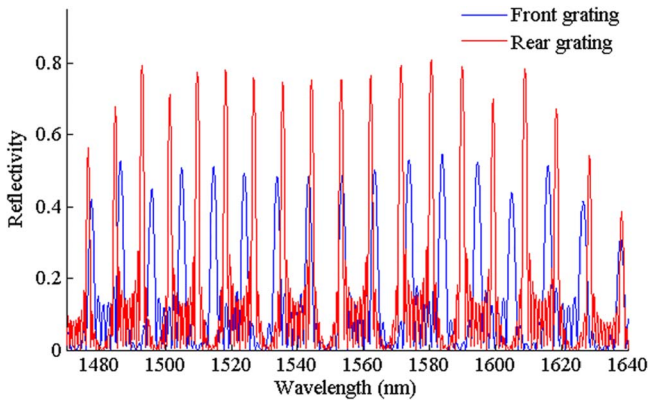

Fig. 6. Reflectivities of the front and rear MPS-DCGs.

TABLE 3

Material parameters used in simulation

Parameters		Symbol	Values
Waveguide thickness	Active section	d (μm)	0.18
	Passive section	d_p (μm)	0.23
Waveguide width		W (μm)	1.2
Waveguide loss		α_0 (cm^{-1})	20
Optical confinement factor		Γ	0.3
Effective refractive index		n_{eff0}	3.23
Group refractive index		n_g	3.72
Transparent carrier density		N_{tr} (cm^{-3})	1.5×10^{18}
Differential gain coefficient		g_N (cm^2)	3×10^{-16}
Carrier life time		τ (s)	1×10^{-8}
Bimolecular recombination coefficient		B (cm^3/s)	10^{-10}
Auger ecombination coefficient	Active section	C (cm^6/s)	4×10^{-29}
	Passive section	C_p (cm^6/s)	7.5×10^{-29}
Nonlinear gain coefficient		ε (cm^3)	1.5×10^{-17}

Fig. 7(a) and (b) show the wavelength and the SMSR tuning curves as a function of the currents across the front and rear grating sections, respectively. The active and phase sections are biased at 75 mA and 0 mA, respectively. As shown in Fig. 7(a), by tuning the front current from 0 mA to 30 mA, the mode hops to higher wavelength, after that a cycle jump of the lasing wavelength from

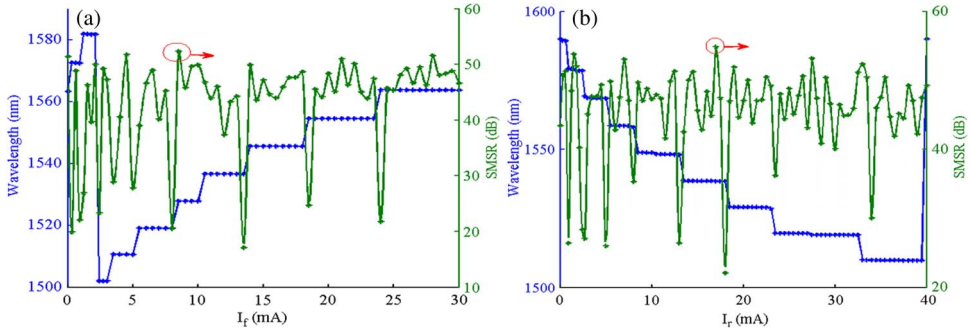

Fig. 7. Tuning curves of: (a) front grating section, with $I_r = 29.5$ mA; (b) rear grating section, with $I_f = 6$ mA.

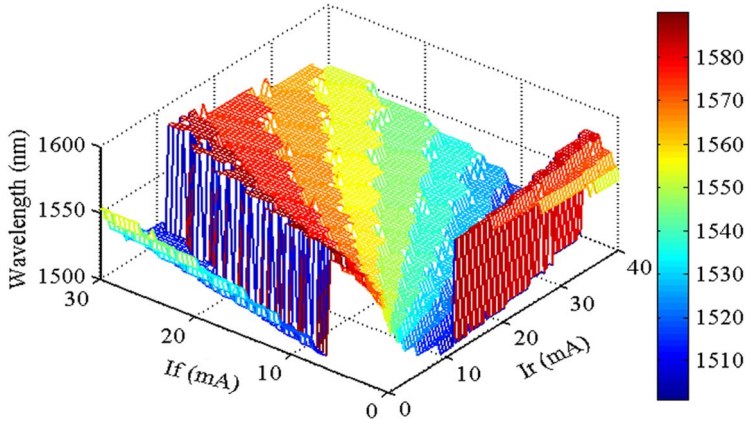

Fig. 8. Three-dimension wavelength tuning map.

1581.8 to 1502 nm is observed. The mode hop spacing is about 8.9 nm, which is approximately equal to the peak spacing of rear grating due to the Vernier tuning mechanism [4]. In a similar way, by tuning the rear current from 0 mA to 40 mA, the mode hops to lower wavelength, and a wavelength cycle jump from 1509.8 to 1589.9 nm is observed with a mode spacing of around 9.9 nm, which is approximately equal to the peak spacing of the front grating. It is clear in Fig. 7(a) and (b) that the good SMSR (> 40 dB) can be achieved in the center area of each mode, while SMSR decreases at the mode boundaries. The 3-D wavelength tuning map is plotted in Fig. 8. It shows that the maximum tuning range of the device is approximately 90 nm, covering a wavelength range from 1500 nm to 1590 nm, which is slightly larger than the designed value.

As shown in Fig. 9, when the active section and phase section are biased at 75 mA and 0 mA, respectively, by tuning the current applied on the front and rear grating sections, the output power from the front MPS-DCG section facet varies from approximately 7.5 dBm to 10.8 dBm, which is predicted to be larger than that of the SG-DBR lasers [4]. This is because that a shorter grating is needed to provide sufficient high reflectivity for the MPS-DCG, and thus reducing optical loss in front section. However, as the thermal effects are not included in this model, the output power might be overestimated, especially when large current is injected into the active section. This is because that with the increasing of the active region current, the active region temperature increases as well, and the leakage and nod-radiative combination become more significant, which reduce the output power. Since the output optical field has to pass through the front MPS-DCG section, this causes a power variation of 3.3 dB when increasing the injected currents in grating sections. A SOA integrated in the front MPS-DCG section could reduce output power variation and improve the output power further.

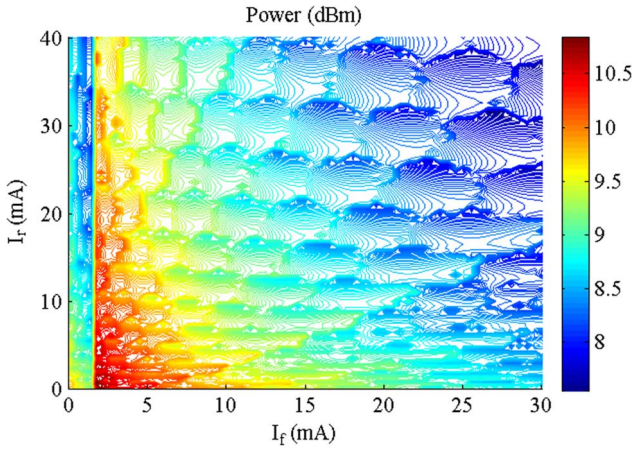

Fig. 9. Contour of the output power.

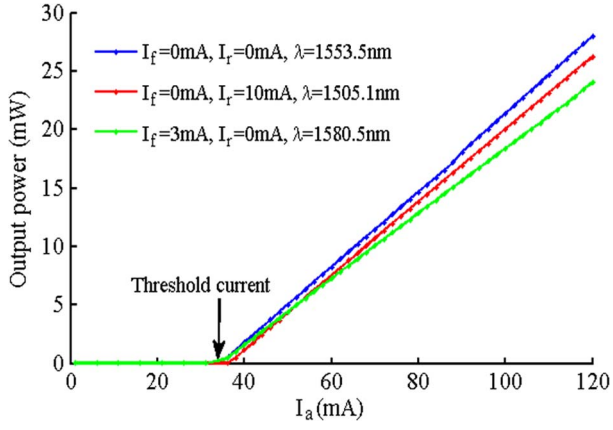

Fig. 10. P-I curves of the MPS-DCG DBR laser.

In Fig. 10, the light output power is shown for three wavelength channels as a function of the current injected on active section. No kinks are observed over the tuning range from 40 mA to 120 mA. The results indicate that the threshold currents of the three different wavelengths are around 33 mA. We attribute this to the relatively low reflectivity of the front grating section as shown in Fig. 6. By increasing the reflectivity of the front MPS-DCG, the threshold current could be reduced as well as the output power. Therefore, a design tradeoff is found between the threshold current and the output power of the laser.

4. Conclusion

We have proposed a new widely tunable DBR laser based on digital concatenated grating with multiple phase shifts. The static characteristics of the MPS-DCG DBR laser were analyzed. The tuning range of the laser was approximately 90 nm, while maintaining a high SMSR (> 40 dB) in the center of each mode. As the MPS-DCG has a high reflection efficiency, short gratings are needed to provide enough reflectivity. High output power could be easily obtained. Moreover, the MPS-DCG can be applied to other laser structures such as the GCSR laser or the DS-DBR laser as it can produce broadband periodic multiple high reflection peaks with a simple structure. These results show that the proposed device could be a promising candidate for future tunable laser sources.

References

[1] L. A. Coldren, G. A. Fish, Y. Akulova, J. S. Barton, L. Johansson, and C. W. Coldren, "Tunable semiconductor lasers: A tutorial," *IEEE J. Lightw. Technol.*, vol. 22, no. 1, pp. 193–202, Jan. 2004.

[2] T. Day, C. B. Thompson, and J. Lee, "Widely tunable laser technologies: Meeting the needs of tomorrow's networks," in *Proc. SPIE*, 2002, vol. 4652, pp. 186–196.

[3] J. Buus and E. J. Murphy, "Tunable lasers in optical networks," *IEEE J. Lightw. Technol.*, vol. 24, no. 1, pp. 5–11, Jan. 2006.

[4] V. Jayaraman, Z. M. Chuang, and L. A. Coldren, "Theory, design, and performance of extended tuning range semiconductor lasers with sampled gratings," *IEEE J. Quantum Electron.*, vol. 29, no. 6, pp. 1824–1834, Jun. 1993.

[5] Y. Tomori, Y. Yoshikuni, H. Ishii, F. Kano, T. Tamamura, Y. Kondo, and M. Yamamoto, "Broad-range wavelength-tunable superstructure grating (SSG) DBR lasers," *IEEE J. Quantum Electron.*, vol. 29, no. 6, pp. 1817–1823, Jun. 1993.

[6] O. A. Lavrova and J. Blumenthal, "Detailed transfer matrix method-based dynamic model for multisection widely tunable GCSR lasers," *IEEE J. Lightw. Technol.*, vol. 18, no. 9, pp. 1274–1283, Sep. 2000.

[7] A. J. Ward, D. J. Robbins, G. Busico, E. Barton, L. Ponnampalam, J. P. Duck, N. D. Whitbread, P. J. Williams, D. C. J. Reid, A. C. Carter, and M. J. Wale, "Widely tunable DS-DBR laser with monolithically integrated SOA: Design and performance," *IEEE J. Sel. Topics Quantum Electron.*, vol. 11, no. 1, pp. 149–156, Jan./Feb. 2005.

[8] G. Sarlet, G. Morthier, R. Baets, D. J. Robbins, and D. C. J. Reid, "Optimization of multiple exposure gratings for widely tunable lasers," *IEEE Photon. Technol. Lett.*, vol. 11, no. 1, pp. 21–23, Jan. 1999.

[9] A. J. Ward, D. J. Robbins, D. C. J. Reid, N. D. Whitbread, G. Busico, P. J. Williams, J. P. Duck, D. Childs, and A. C. Carter, "Realization of phase grating comb reflector and their application to tunable DBR lasers," *IEEE Photon. Technol. Lett.*, vol. 16, no. 11, pp. 2427–2429, Nov. 2004.

[10] I. A. Avrutsky, D. S. Ellis, A. Tager, H. Anis, and J. M. Xu, "Design of widely tunable semiconductor lasers and the concept of binary superimposed gratings (BSG's)," *IEEE J. Quantum Electron.*, vol. 34, no. 4, pp. 729–741, Apr. 1998.

[11] J. O. Wesström, G. Sarlet, S. Hammerfeldt, L. Lundqvist, P. Szabo, and P. J. Rigole, "State-of-the-art performance of widely tunable modulated grating Y-branch lasers," presented at the Proc. Opt. Fiber Commun. Conf., Los Angeles, CA, USA, 2004, Paper TuE2.

[12] X. Y. He, D. X. Huang, Y. L. Yu, D. N. Wang, W. Liu, and S. Jiang, "Widely wavelength-selectable lasers with digital concatenated grating reflectors-proposal and simulation," *IEEE Photon. Technol. Lett.*, vol. 20, no. 21, pp. 1754–1756, Nov. 2008.

[13] N. Yusuke and Y. Shinji, "Densification of sampled fiber Bragg gratings using multiple-phase-shift (MPS) technique," *IEEE J. Lightw. Technol.*, vol. 23, no. 4, pp. 1808–1817, Apr. 2005.

[14] Y. C. Tang, J. L. Zhao, Y. W. Zhang, Y. L. Yu, N. Zhou, and W. Liu, "Fabrication of digitally concatenated gratings using nanoimprint lithography," *Optics. Prec. Eng.*, vol. 19, no. 7, Jul. 2011.

[15] J. L. Zhao, Y. L. Yu, and Y. C. Tang, "Design of high channel-count comb filter based on digital concatenated grating with multiple phase shifts (MPS-DCG)," *IEEE Photon. Technol. Lett.*, vol. 23, no. 23, pp. 1814–1816, Dec. 1, 2011.

[16] L. M. Zhang, S. F. Yu, M. C. Nowell, D. D. Marcenac, J. E. Carroll, and R. G. S. Plumb, "Dynamic analysis of radiation and side-mode suppression in a second-order DFB laser using time-domain large-signal traveling wave model," *IEEE J. Quantum Electron.*, vol. 30, no. 6, pp. 1389–1395, Jun. 1994.

[17] W. Li, W.-P. Huang, and X. Li, "Digital filter approach for simulation of a complex integrated laser diode based on the traveling-wave model," *IEEE J. Quantum Electron.*, vol. 40, no. 5, pp. 473–480, May 2004.

[18] L. Dong, R. Zhang, D. Wang, S. Zhao, S. Jiang, Y. Yu, and S. Liu, "Modeling widely tunable sampled-grating DBR lasers using traveling-wave model with digital filter approach," *IEEE J. Lightw. Technol.*, vol. 27, no. 15, pp. 3181–3188, Aug. 2009.